

AD-A031 808

MICHIGAN TECHNOLOGICAL UNIV HOUGHTON

RELATION BETWEEN ELECTRONIC STRUCTURE AND THE MECHANICAL PROPER--ETC(U)

JUN 76 D F STEIN, G W SHANNETTE

DA-ARO-D-31-124-72-G38

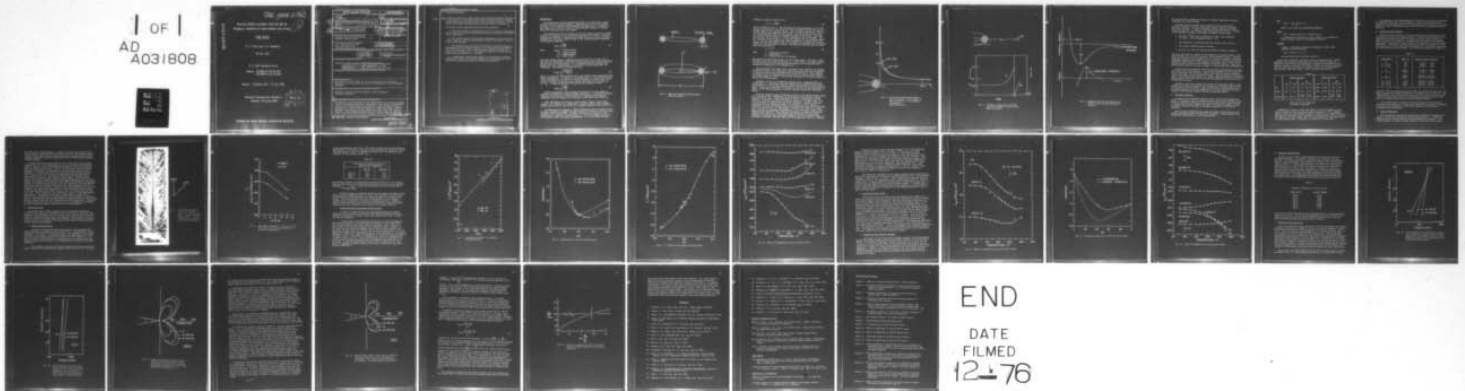
F/G 11/6

NL

UNCLASSIFIED

ARO-10453.2-MC

1 OF 1
AD
A031808



END

DATE
FILMED
12-76

ADA031808

ARO-10453.2-0aC^{FG}

RELATION BETWEEN ELECTRONIC STRUCTURE AND THE
MECHANICAL PROPERTIES OF BODY-CENTERED CUBIC METALS

12

FINAL REPORT

D. F. STEIN AND G. W. SHANNETTE

30 JULY 1976

U. S. ARMY RESEARCH OFFICE

GRANTS: DA-AROD-31-124-72-G38
DA-AROD-31-124-73-G142

PERIOD: 1 OCTOBER 1971 - 31 JULY 1976

MICHIGAN TECHNOLOGICAL UNIVERSITY
HOUGHTON, MICHIGAN 49931

DDC
RECEIVED
NOV 10 1976
A

APPROVED FOR PUBLIC RELEASE; DISTRIBUTION UNLIMITED.

| REPORT DOCUMENTATION PAGE | | READ INSTRUCTIONS BEFORE COMPLETING FORM |
|---|-----------------------|--|
| 1. REPORT NUMBER 10453MS | 2. GOVT ACCESSION NO. | 3. RECIPIENT'S CATALOG NUMBER ⑨ |
| 4. TITLE (and Subtitle) RELATION BETWEEN ELECTRONIC STRUCTURE AND THE MECHANICAL PROPERTIES OF BODY-CENTERED CUBIC METALS. | | 5. TYPE OF REPORT & PERIOD COVERED Final Report. 1 October 1971-31 July 1976, |
| 7. AUTHOR(s) D. F. Stein G. W. Shannette | | 6. PERFORMING ORG. REPORT NUMBER |
| 9. PERFORMING ORGANIZATION NAME AND ADDRESS Michigan Technological University Houghton, Michigan 49931 | | 8. CONTRACT OR GRANT NUMBER(s) DA-AROD-31-124-72-G38, Add DA-AROD-31-124-73-G142 |
| 11. CONTROLLING OFFICE NAME AND ADDRESS U. S. Army Research Office Post Office Box 12211 Research TRIangle Park, NC 27709 | | 10. PROGRAM ELEMENT, PROJECT, TASK AREA & WORK UNIT NUMBERS |
| 14. MONITORING AGENCY NAME & ADDRESS (if different from Controlling Office) ⑫ 35p. | | 12. REPORT DATE 30 June 1976 |
| | | 13. NUMBER OF PAGES 32 |
| | | 15. SECURITY CLASS. (of this report) Unclassified |
| | | 15a. DECLASSIFICATION/DOWNGRADING SCHEDULE |
| 16. DISTRIBUTION STATEMENT (of this Report) Approved for public release; distribution unlimited. ⑱ ARD ⑲ 10453.2-MC | | |
| 17. DISTRIBUTION STATEMENT (of the abstract entered in Block 20, if different from Report) | | |
| 18. SUPPLEMENTARY NOTES The findings in this report are not to be construed as an official Department of the Army position, unless so designated by other authorized documents. | | |
| 19. KEY WORDS (Continue on reverse side if necessary and identify by block number) Electronic Structure, Brittle Fracture, Elastic Constants, Mechanical Properties | | |
| 20. ABSTRACT (Continue on reverse side if necessary and identify by block number) The objective of this program was the understanding of the role of alloying elements in promoting ductility in BCC metals. The program considered the roles of both increased cohesive strength of solids and enhanced plastic deformation in improving the resistance of a solid to fracture. Various approaches were used to evaluate changes that could affect the fracture behavior. These included estimates of true surface energy and fracture stress using interatomic potential functions, and the effect (continued) → next page | | |

20. Abstract (continued)

cont.

→ of plastic deformation using a model crack that allowed plastic deformation at the crack tip. Measurements were made of elastic constants, magnetic susceptibility, and fracture energies of pure metals and alloys. Several alloys were studied including Fe-Si, W-Re, W-Ta, Nb-Zr, and Nb-Hf. ↗

The results can be summarized and generalized as follows:

1. The fracture plane is determined by the rate of plastic deformation at the crack tip, with the (100) plane having the minimum plastic deformation in BCC metals.

2. The surface energy of BCC metals as determined by using the interatomic potential function suggested by Mie, Morse, and Johnson. They all predict (110) cleavage.

3. The stability and ductility of BCC metals are directly related to the magnitude of the elastic constant, $C' = 1/2(C_{11}-C_{12})$ and BCC metals, with large values of C' tend to be more stable and more brittle than metals with low values of C' . This implies a maximum in d-electron type bonding when the ductility is a minimum.

4. A model which involves both changes in the theoretical cohesive strength and changes in dislocation mobility was developed that is consistent with the observed changes in mechanical properties.

| | |
|----------------------------------|---|
| ACCESSION No. | |
| NTIS | Write Section <input checked="" type="checkbox"/> |
| BCC | Self Service <input type="checkbox"/> |
| UNANNOUNCED | <input type="checkbox"/> |
| AUTHORITY | |
| BY | |
| DISSEMINATION AVAILABILITY CODES | |
| REMARKS (SEE END OF SPECIAL) | |
| A | |

Introduction

The experimental program described here had as its objective to understand the role of alloying elements in promoting ductility in BCC metals. In order to understand why each measurement was made and how it related to this objective, it would be useful to first describe a model of fracture which has developed during this program.

The problem with brittle fracture is the low stresses required to induce fracture in comparison to the theoretical strength of a crystal. Griffith¹ developed the approach of balancing the energy required to form new fracture surfaces with the elastic energy stored in the strained material resulting in the familiar equation,

$$\sigma_{\text{Frac}} = \sqrt{\frac{2E\gamma}{\pi c}} \quad (1)$$

where

- σ_{Frac} = Fracture Stress
- E = Young's Modulus
- γ = Surface Energy
- 2c = Crack Length

This model proved useful in explaining why materials were so weak, but it was found that most metals exhibited fracture energies that were considerably greater than the surface energy. As a consequence Orowan² proposed that a plastic work term, represented as an artificial surface energy term, be introduced. The resulting equation was then

$$\sigma_{\text{Frac}} = \sqrt{\frac{2E(\gamma_s + \gamma_p)}{\pi c}} \quad (2)$$

where γ_s is the true surface energy and γ_p the surface energy associated with plastic deformation. In general, it was found that $\gamma_s \ll \gamma_p$ and this had led to the development of the field of fracture mechanics in which Irwin³ first defined a term G_c , called the energy release rate which is just equal to $\gamma_s + \gamma_p$. In fracture mechanics the equation for fracture is then

$$\sigma_{\text{Frac}} = \sqrt{\frac{2EG_c}{\pi c}} \quad (3)$$

Further development of this equation has proven to be very useful in selecting materials for a specific design application. In fracture mechanics language, the objective of this program is to understand what physical properties that are changed during alloying of BCC metals that affect G_c .

Since the plastic work term γ_p is much greater than γ_s , γ_s is often ignored. This appears to be unfortunate, because a rather simple argument reveals that γ_p can be, and usually is, strongly affected by the value of γ_s .

To demonstrate the argument, a model developed by Hahn and Gilbert⁴ will be used, followed by arguments by Ayres and Stein⁵ and Tyson, Ayres and Stein⁶ developed under this program. Consider a sharp crack of length c with a plastic zone of radius r as shown in Fig. 1. If it is assumed that this is an elliptical crack, the stress concentration, α^* , at the elastic-plastic

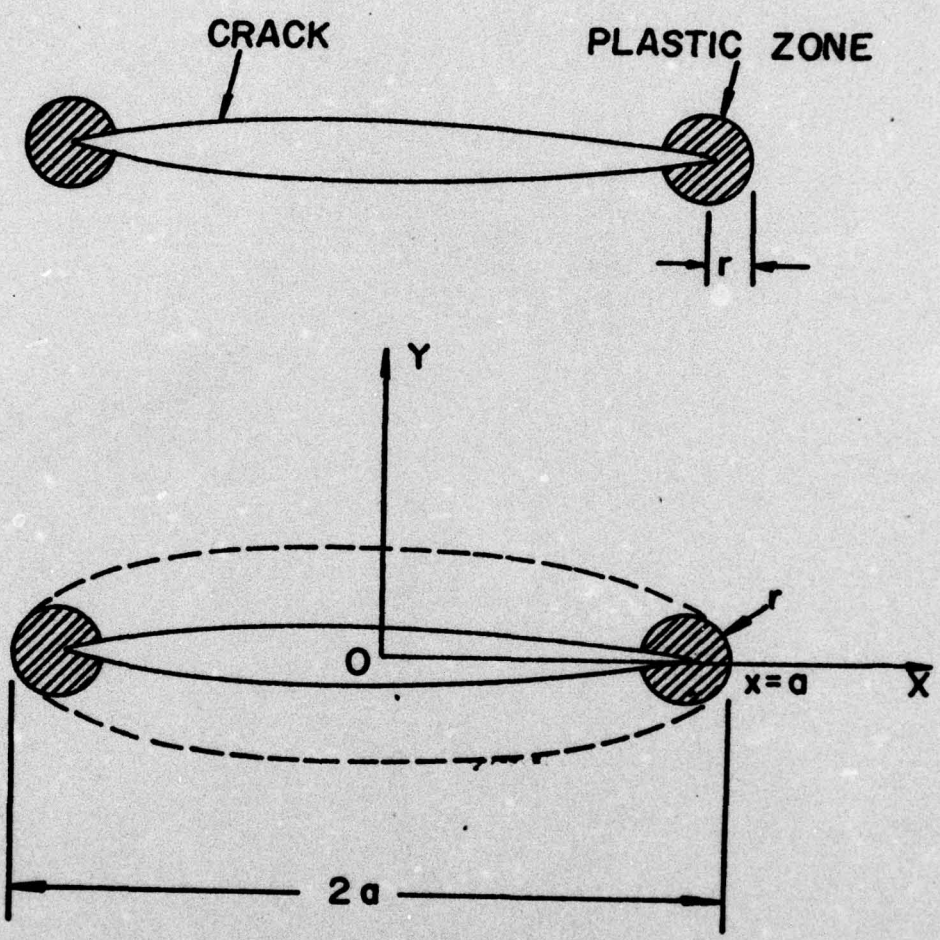


Fig. 1. Model of a Partially Relaxed Crack.
Hahn and Gilbert⁴

boundary is given by Inglis⁷ to be

$$\alpha^* = 1 + 2\sqrt{a/r} \quad (4)$$

and it is shown in Fig. 2. The condition for crack propagation is that the stress concentration at the crack tip times the nominal stress ($\alpha^* \sigma_{nom}$) be greater than the true fracture stress. This is shown schematically in Fig. 3. In this figure taken from Hahn and Gilbert,⁴ the stress and strain history of a volume element ahead of a propagating crack is calculated. Now there are two ways that the amount of plastic deformation can be increased. One can lower the yield stress, σ_y , or one can increase the true fracture stress, σ^* . At first it might appear that small increases in σ^* would have little effect, but one must remember that in BCC metals the dependence of dislocation velocity is very dependent on stress. The empirical relation used to relate these two quantities is

$$v = A \tau^m \quad (5)$$

where v = dislocation velocity
 τ = shear stress
 m = dislocation velocity exponent

The values of m range from around 7 to 40 for BCC metals. Therefore a small increase in the true fracturing stress, σ^* , could result in a large increase in the plastic work since the maximum shear stress at the crack tip will increase in proportion to the increase in σ^* .

Ayres and Stein⁵ and Tyson, Ayres, and Stein⁶ have developed the approach of Hahn and Gilbert⁴ for crystalline materials and they have been successful in predicting the correct cleavage planes in BCC materials. Their argument is basically that the cleavage plane is the plane of fracture which induces the minimum amount of plastic work and that in general it is not the plane of lowest true surface energy.

Therefore, if one is to understand fracture from a crystallographic or atomic basis, it is necessary that one understand the interrelation between the cohesion of a solid (true fracture stress) and dislocation motion (plastic work). If one is to understand the effect of alloying, one must determine the effect of the alloying element on both the cohesive stress and dislocation motion.

Since the cohesive stress is directly related to the binding between atoms, it is necessary that a formulation of the attractive and repulsive forces between atoms be made. These relations are known as interatomic potential functions. However, the nature of metallic binding is so complex that it is not now possible to derive them from first principles. However, using the convention that the potential energy of the system is zero at infinite separation of atoms, the general shape of the potential curve can be concluded to be that shown in Fig. 4. The energy is negative over most of its range, with a minimum at the equilibrium spacing x_0 . The force curve shown in Fig. 4 represents the external force which must be applied to produce a separation between atoms equal to x . This maximum force represents the theoretical strength of the solid and is directly related to the true fracture stress, σ^* , previously discussed. The area under the force-separation curve is a measure

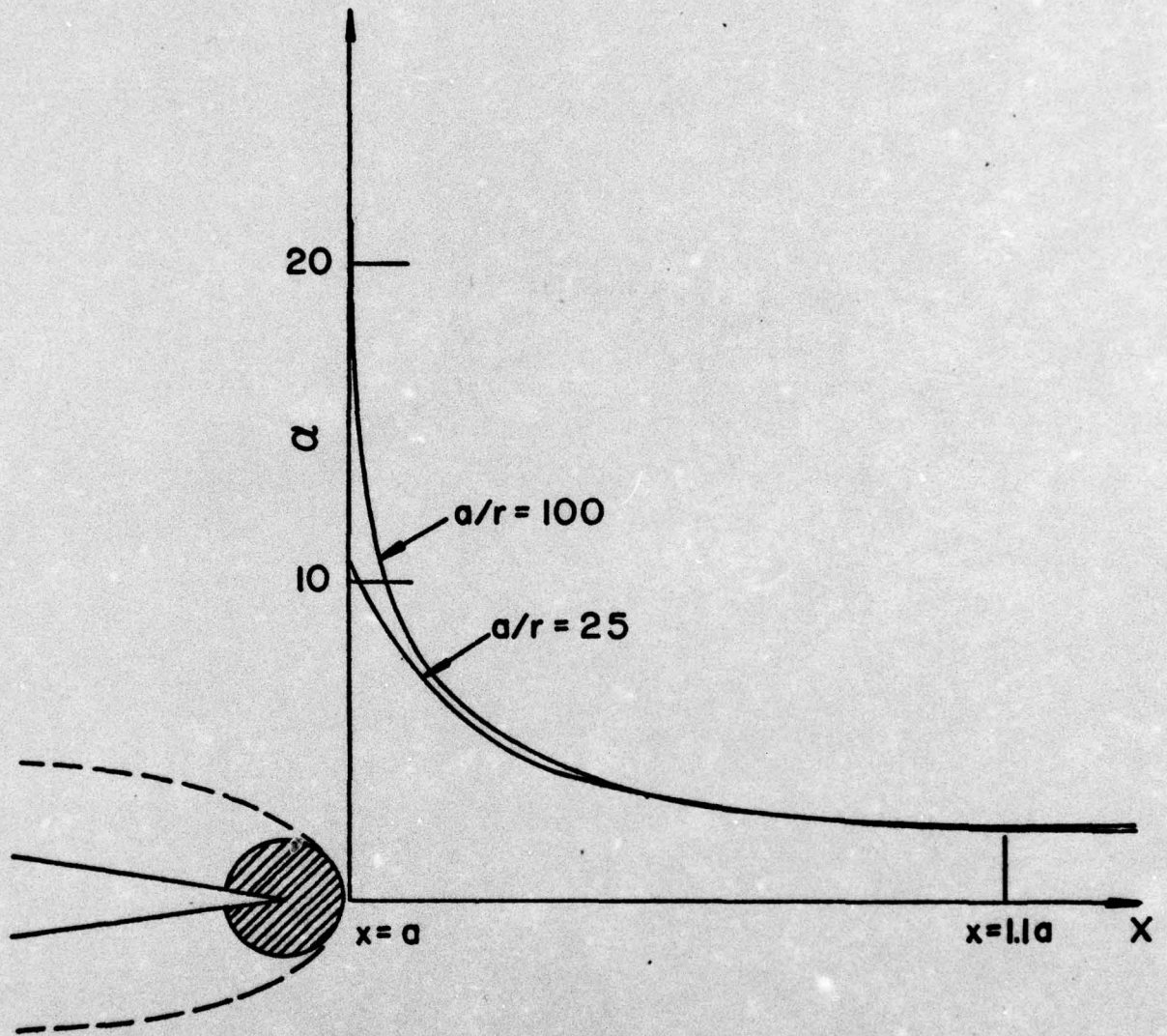


Fig. 2. Calculated Stress Concentration α for an Elliptical Crack, Length $2a$ and Root Radius r , as a Function of Distance.
Hahn and Gilbert⁴

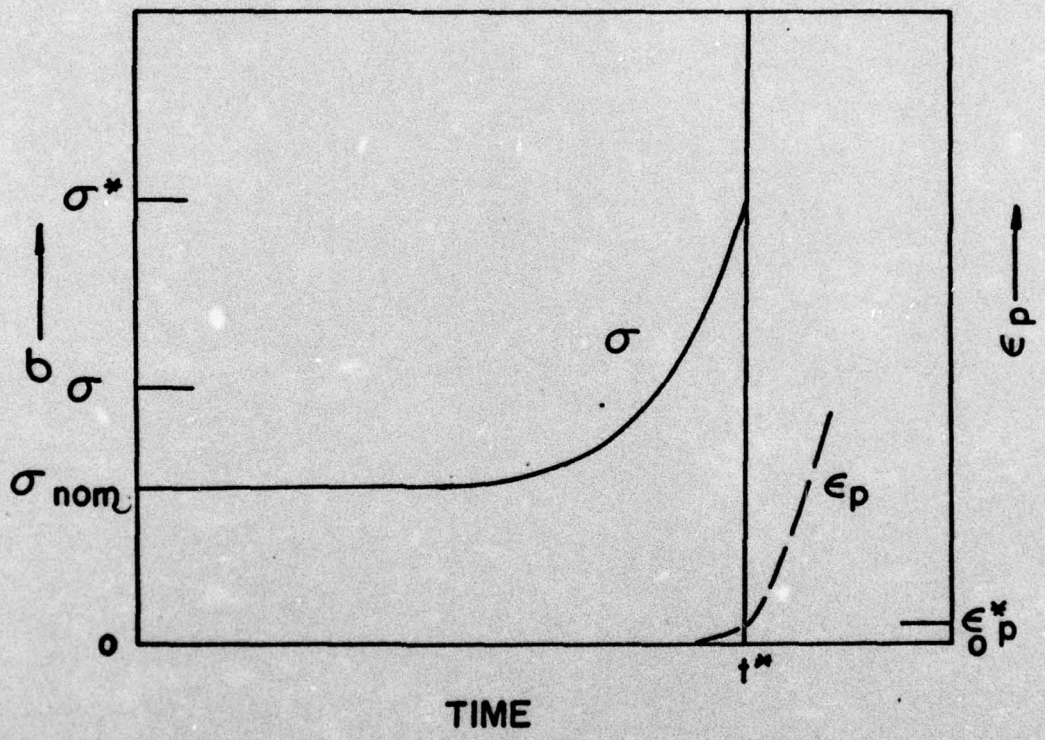
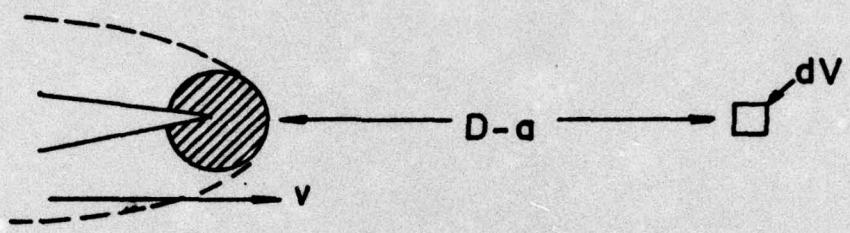


Fig. 3. Schematic Presentation of Stress and Strain Ahead of a Moving Crack. Hahn and Gilbert⁴

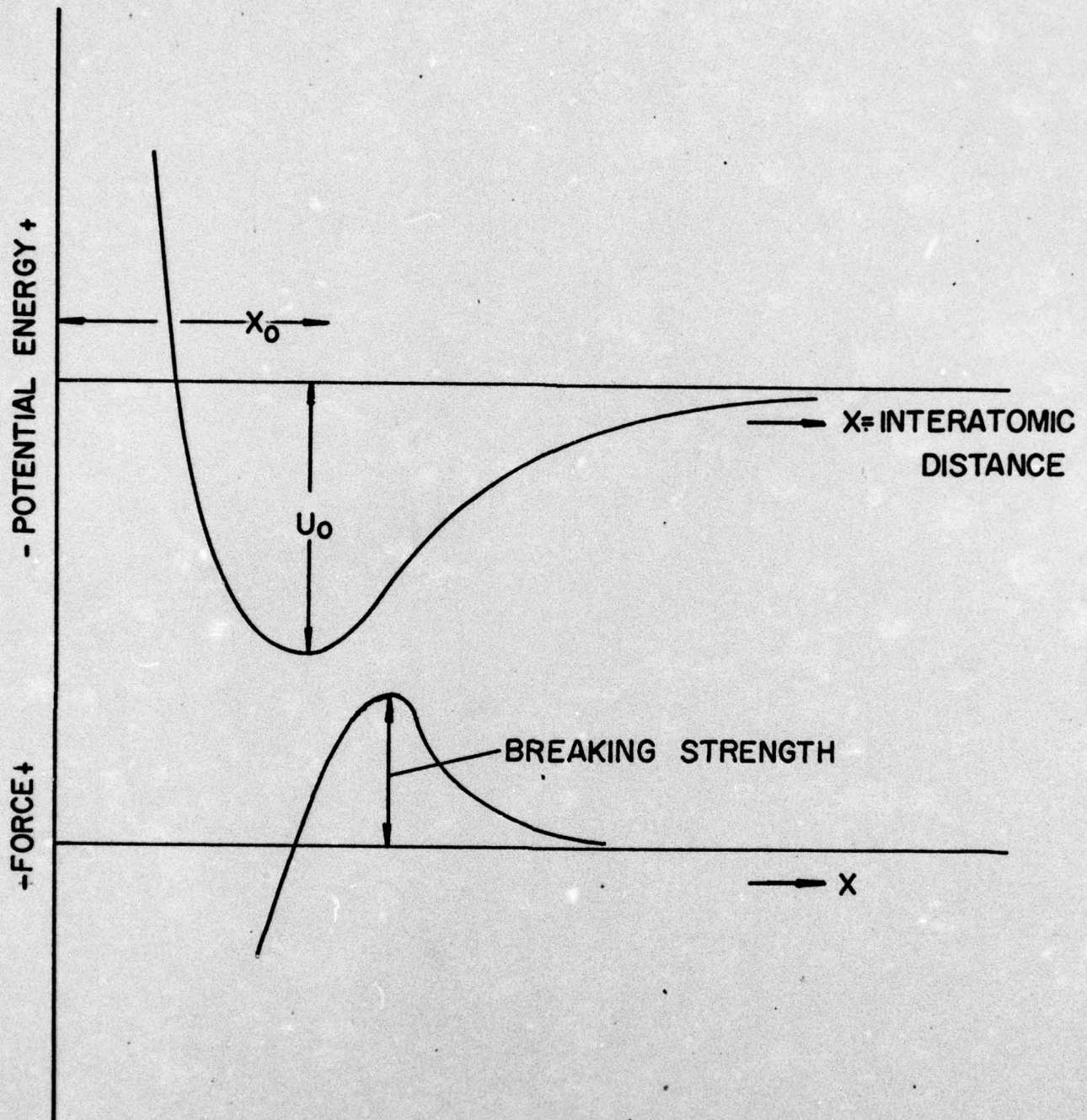


Fig. 4. Schematic of Potential Function and Force Function for One-Dimensional Crystal.

of the work done to separate two atoms to infinite separation, and thus represents the surface energy.

Although metallic bonding is too complex to allow calculation of potential functions from first principles, various empirical functions have been suggested. In order to represent atomic interactions within a stable crystal, any such function must satisfy certain criteria. If $\phi(r)$ is the interaction energy of two atoms a distance r apart, then:

1. The force $-\frac{d\phi}{dr}$ must be repulsive at small r and attractive at large r , with a minimum at some $r = r_0$.
2. The magnitude of ϕ must decrease more rapidly with r than r^{-3} .
3. The elastic constants must be positive.
4. $C_{11} - C_{12} > 0$, where C_{11} and C_{12} are elastic stiffness constants.

The first condition is a result of the existence of condensed phases. The second assures that the function gives a finite cohesive energy. Together, these two conditions give a crystal that is stable with respect to infinite homogeneous expansion and contraction of the lattice. The third and fourth conditions, which apply to cubic crystals, have been given by Born⁶ and his associates after analysis of the stability of crystal lattice. These conditions assure that the lattice is stable to infinitesimal shear deformations.

Various empirical potential functions have been developed and three have been used in this investigation. The various parameters in these functions can be determined since they must predict correctly the elastic constants, lattice constants, and the sublimation energy. Other experimental quantities such as the stacking fault energy, the vacancy formation energy, and radiation damage energies have been used to evaluate the parameter for other parts of the potential function.

Therefore, there were several quite different measurements made in this program in an effort to determine the relation the electronic structure has to the ductility of BCC metals. Each of these sets of measurements will be described separately, with an explanation of why they were made, and then related to the fracture behavior through the preceding model.

A. Potential Functions

In order for any potential function to be of value in determining the affect of alloying on the true fracture stress, that function should be able to give a reasonable estimate of the fracture strength for a pure material. It should also be able to predict the value of the surface energy, as this is closely related to the ease of fracture, especially in very brittle materials.

Three potential functions were chosen for study in this portion of the program, the Mie,⁹ Morse¹⁰ and Johnson¹¹ potentials. These functions are represented mathematically in the following way:

Mie

$$\phi(r) = -\frac{A}{r^m} + \frac{B}{r^n} \quad (m < n)$$

where A, B, m and n are adjustable parameters.

Morse

$$\phi(r) = D[\exp(-2\alpha(r-r_0)) - 2 \exp(-\alpha(r-r_0))]$$

D = dissociation energy $\phi(r) = \phi(r_0)$, where $r = r_0$ defined by energy minimum, and α is an adjustable parameter.

Johnson

Johnson's interaction potential is composed of three cubic equations, each of the form

$$\phi(r) = A(r-B)^3 + C r + D$$

and each valid over a specific range of r.

Using elastic constant, sublimation energy, compressibility, thermal expansion and radiation damage data and in some cases the affect of temperature and pressure, the appropriate constants were defined for each function (details in Musolff M.S. Thesis). Using the developed equations, the fracture stress and energy was calculated for iron and tungsten on both the (100) and (110) planes. Table I presents the results.

Table I

| | Fracture Stress* | | | | Fracture Energy** | | | |
|---------|------------------|-------|-------|-------|-------------------|-------|-------|-------|
| | W | | Fe | | W | | Fe | |
| | (100) | (110) | (100) | (110) | (100) | (110) | (100) | (110) |
| Mie | 3.76 | 3.55 | 1.07 | 1.01 | 2600 | 2360 | 784 | 716 |
| Morse | 2.95 | 2.75 | 1.47 | 1.39 | 3870 | 3820 | 1742 | 1806 |
| Johnson | 15.27 | 14.40 | 5.46 | 5.14 | 3690 | 3450 | 1300 | 1200 |
| | | | 5.08 | 4.79 | | | 1030 | 990 |

*In units of 10^{11} dynes/cm²

**In units of ergs/cm²

Examination of Table I shows that there is a wide discrepancy in the fracture stress calculated using the various potentials, with a somewhat smaller variation in the fracture energies. However, it is interesting to note that all potential functions predict that the fracture stress and energy is greater on the (100) plane. This is in contradiction to the observation that BCC metals prefer, in general, to cleave on the (100) plane.

The weakness in our understanding of the bonding in solids as represented by interatomic potentials is very apparent. This is an area deserving of attention by solid state theorists and understanding the cohesion of even pure metals will await development of more rigorously based interatomic potential functions.

B. Fracture Surface Energies

One of the major activities of this program was the measurement of fracture energies in pure and alloyed crystals. The technique was basically one developed by Beardmore and Hull¹² in which they used a spark discharge to induce a crack into a material. The modification included using a greater power input into the crystal and performing the discharge at liquid nitrogen temperature. Specimens of various crystal orientation and composition were then fractured in tension and from the measured load and original crack shape the fracture energy was determined. The results are summarized in Table II.

Table II

| <u>Composition</u> | <u>Temp. °K</u> | <u>Fracture Energy (ergs/cm²)</u> |
|--------------------|-----------------|--|
| W | 77°K | 3,800 ± 500 |
| W - 3% Re | 77°K | 6,300 ± 400 |
| W - 10% Re | 77°K | 12,600 ± 1,000 |
| W | 196°K | 71,500 ± 5,000 |
| W - 3% Re | 196°K | 35,000 ± 2,000 |
| W | 298°K | 245,000 ± 10,000 |
| W - 10% Re | 298°K | Twin-matrix Failure |
| Fe - 3% Si | 77°K | 136,000 ± 100,000 |
| Fe - 3% Si | 298°K | 718,000 ± 50,000 |
| Fe - 3% Si | 323°K | 588,000 ± 270,000 |

Except at 77°K for tungsten and its Re alloys the fracture energies are very large indicating the plastic deformation is extensive at the crack tip. The fracture energy of the pure W is the only one that is very close to the predicted fracture energies using the interatomic potential and even in this case it is probably about twice the true fracture energies.

It is noted that Re increases the fracture energy at 77°K very substantially and therefore it is clear that Re enhances the ability of tungsten to resist crack propagation, rather than changing grain morphology or suppressing crack nucleation.

C. Fracture Morphology

After fracturing, the fracture surfaces were examined to determine the plane of fracture and direction of fast crack propagation. In addition features such as microtwinning and "river markings" were observed. Even though attempts were made to induce fracture on other than (100) planes,

the (100) plane remained dominant. The only real deviation was the twin-matrix failure of the W-10% Re alloy tested at 298°K. The fracture surface of the Fe and W base materials showed much greater deformation when tested at higher temperatures which was consistent with the much greater measured fracture energies.

A common observation became known as the "<100> spike" on the single crystals (Fig. 5). It was found that in a <100> direction on the fracture surface, that the surface was smooth and featureless, much like expected from a perfectly brittle solid. In the <110> direction there were strong markings, either due to microtwinning or the tear lines known as "river markings." It appears that the crack in the BCC metals tested runs much more rapidly in the (100) direction in accordance with the prediction of Tyson, Ayres and Stein.⁶ An effort was made to detect "Wallner lines" which would provide conclusive evidence of the shape of the crack front. However, the surface features resulting from microtwinning and "river lines" obscured or obliterated the "Wallner lines" making the measurement impossible. However, the surface markings were in all cases consistent with the position that (100) cracks are heavily favored and that cracks propagate much more rapidly in the <100> direction. Because of the rapid propagation in the <100> direction the crack is left lagging in the <110> direction and the joining of the two fast propagating <100> fronts results in tracing along the <110> direction. This explains the crystallographic nature of river markings and their origin. The preference for (100) cleavage does not appear to be associated in any way with the segregation of alloying elements to specific planes. Auger Electron Spectroscopy studies of cleaved surfaces of many alloys has not revealed other than the expected average bulk composition. Therefore, it appears that the (100) cleavage planes are not an artifact in BCC metals, but the inherent and natural fracture plane for these materials.

D. Elastic Constants

The single crystal elastic constants for the following systems were determined as a function of temperature: W-Re, W-Ta, Nb-Zr, and Nb-Hf. The purpose in obtaining these data was twofold; first, the data were needed to calculate certain parameters such as the apparent surface energies which are useful in evaluating fracture models and secondly, the electronic structure has an effect on the ductility of a metal and this effect may be defined by elastic constant measurements.

1. Tungsten-Rhenium System

The first system measured was W-Re because it is well known that rhenium additions to tungsten increase ductility.¹³ The stability and the ductility of BCC metals are directly related to the magnitude of the elastic constant¹⁴ $C' = 1/2(C_{11} - C_{12})$ and BCC metals with large values of C' tend to be more stable and more brittle than metals with low values of C' . As shown in Fig. 6, rhenium additions to tungsten up to 10 atomic percent were found to decrease the value of C' , thus decreasing the stability of the BCC structure.

In an effort to relate the elastic constants to electronic structure, Fisher and Dever¹⁵ have developed an equation that relates C' with the value

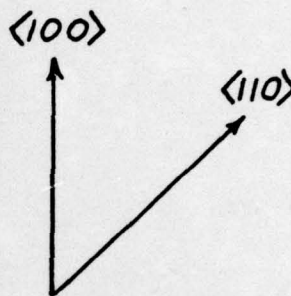
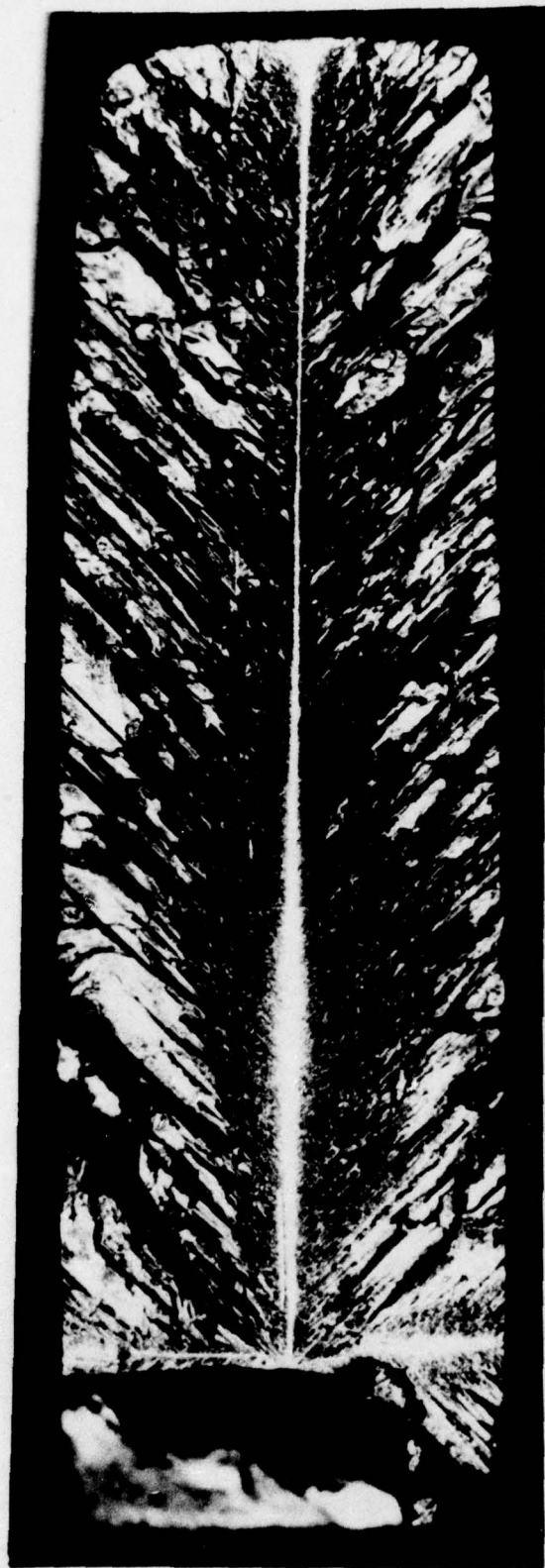


Fig. 5. $\langle 100 \rangle$ Fracture Surface of W-3% Re tested at 298°K . The smooth $\langle 100 \rangle$ spike is shown originating from precrack. Coarse microtwins lay parallel to the $\langle 110 \rangle$ direction.

60X

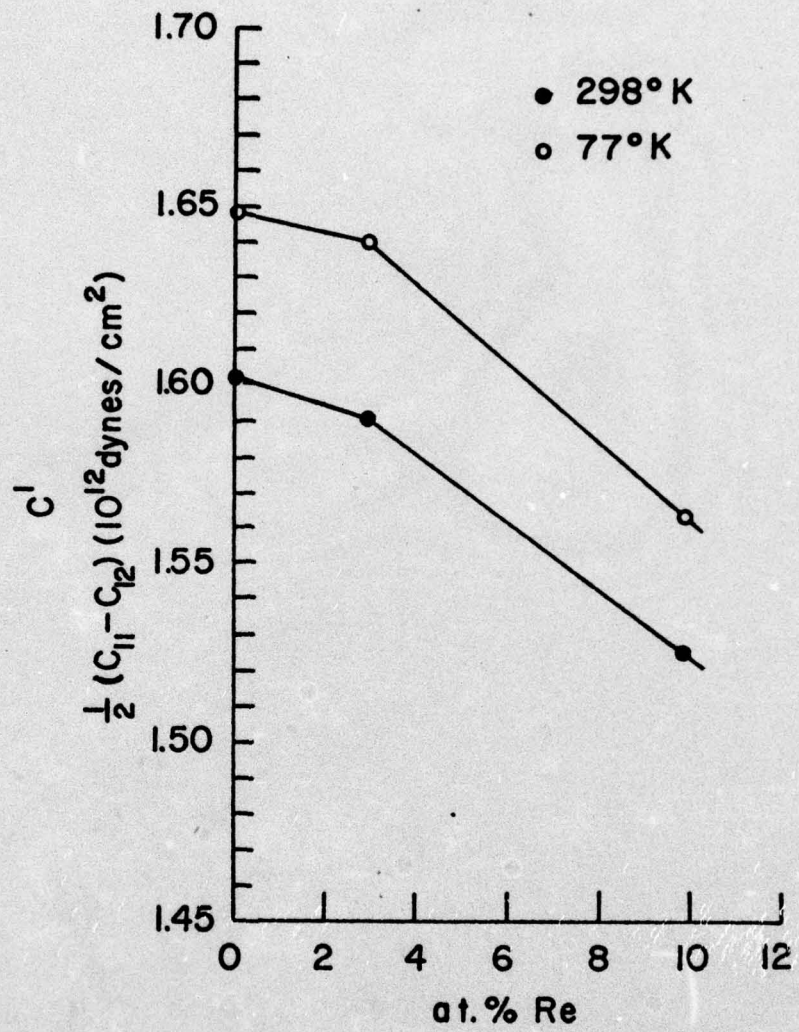


Fig. 6. The elastic constant $C^1 = 1/2 (C_{11} - C_{12})$ as a function of rhenium content for different temperatures.

of the electron/atom ratio (e/a). Their model assumes that the tight bonding approximation is valid and it appears to give satisfactory results for transition metal alloys. Table III contains the values of C' calculated by this technique and the measured values of C' .

Table III

| Calculated and Measured Values of C' (units of 10^{12} dynes/cm ²) | | |
|---|----------------|-----------------|
| | <u>W-3% Re</u> | <u>W-10% Re</u> |
| Calc. C' | 1.56 | 1.47 |
| Meas. C' | 1.59 | 1.52 |
| Error | 1.9% | 3.3% |

The agreement between the calculated and measured values of C' is excellent. However, later work in this study and by Fisher¹⁶ has shown that the elastic anisotropy $\frac{2C_{44}}{(C_{11} - C_{12})}$ is more closely related to the e/a ratio than C' .

$$[A = \frac{2C_{44}}{(C_{11} - C_{12})}]$$

Another attempt at predicting ductility from elastic constants of pure metals was first proposed by Pugh¹⁷ in 1954. He suggested that high ratios of bulk modulus to shear modulus, B/G , correlates well with increasing ductility. In the W-Re system, the ratio of bulk modulus to shear modulus increases with Re additions to W implying increased ductility. However, a lack of correlation between the B/G ratio and ductility in other BCC alloys indicates that this criterion is not sufficient to predict ductility.

2. Niobium-Zirconium and Niobium-Hafnium Systems

In order to further develop the relationship between the elastic constants and the electronic structure of BCC transition metals and alloys, the elastic constants of a Group V metal (Nb) alloyed with Group IV metals (Zr, Hf) were measured.

In this study, it was found that the value of C' does correspond to the value calculated by the Fisher-Dever relationship for the Nb-Zr system but the Nb-Hf values do not show as good an agreement. This is shown in Fig. 7 where the solid lines represent the calculated values. However, it was found that the elastic anisotropy ratio is very closely related to the e/a ratio as shown in Fig. 8. Fisher¹⁶ predicted that the curve of A vs. e/a should be U-shaped with a minimum occurring at a e/a of about 5.5. The values determined in this and in other investigations do exhibit this type of behavior as shown in Fig. 8. The effect of temperature on A was also determined and is shown in Figs. 9 and 10. It can be noted that there is a minimum in the curve for pure Nb and this minimum tends to disappear when either Hf or Zr are added. A complete explanation for this is not available at this time but it is probably related to changes in the Fermi surface that occur with changing temperature.

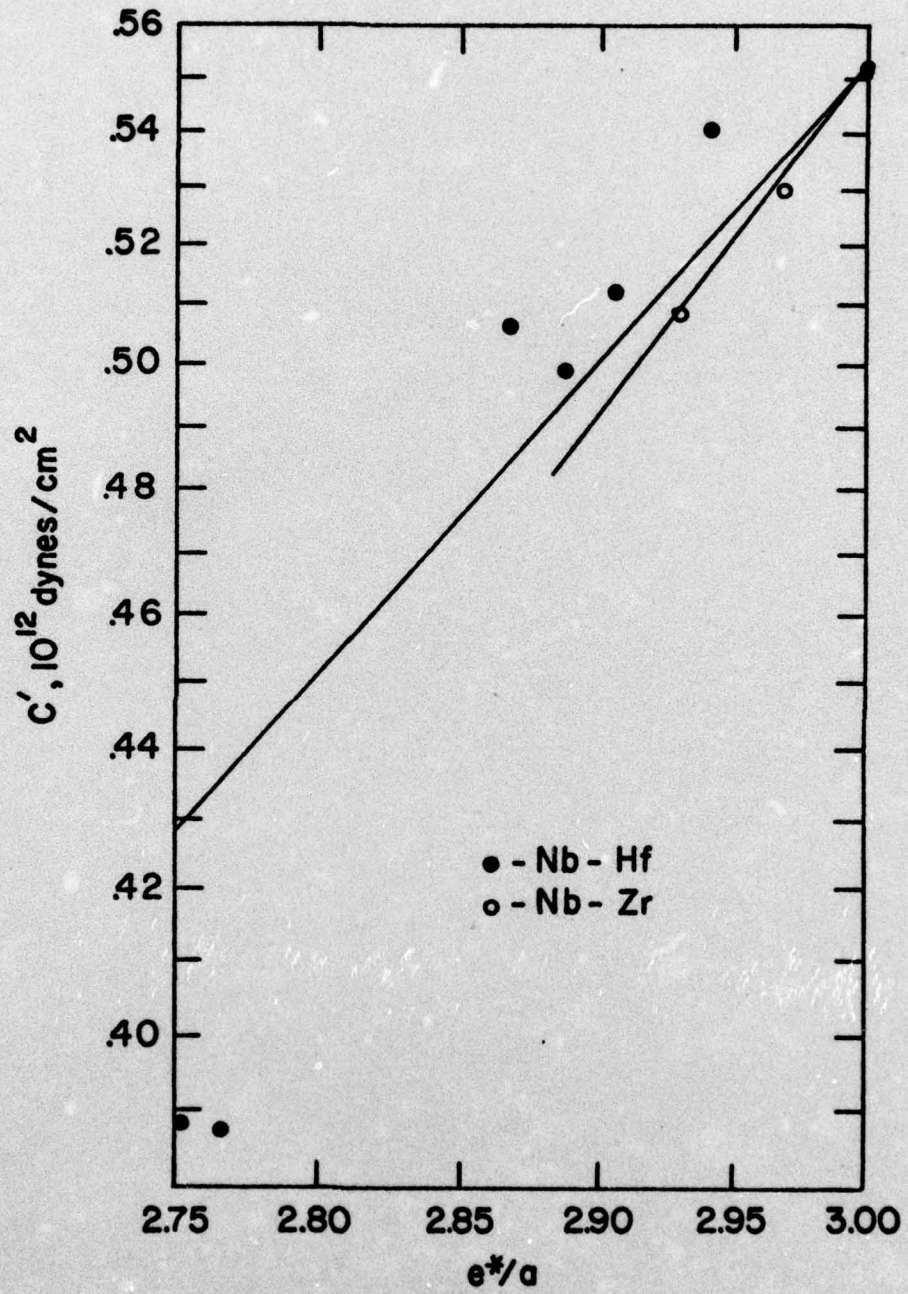


Fig. 7. The Elastic Constant C' for Nb-Hf and Nb-Zr Alloys.

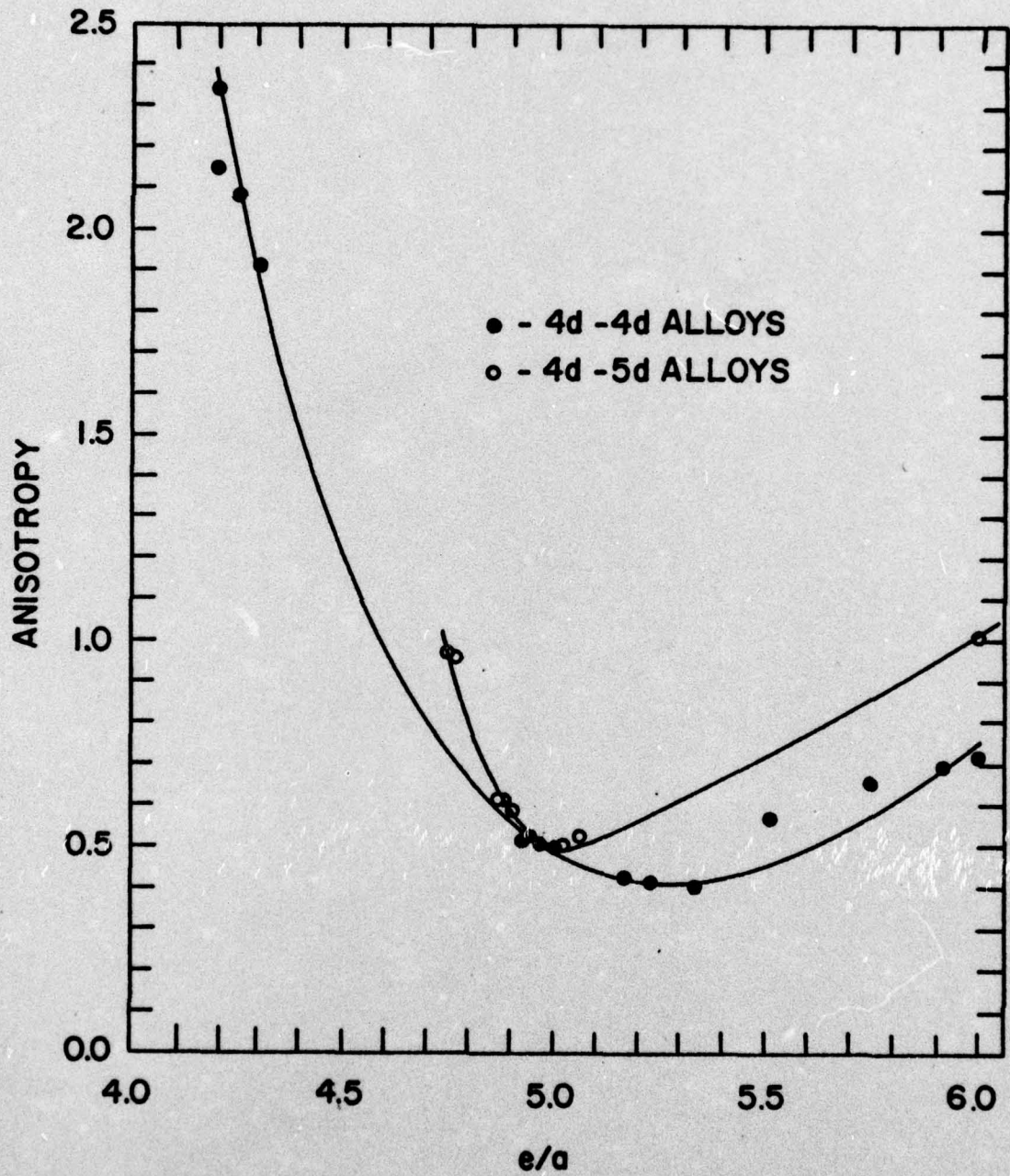


Fig. 8. Anisotropies of 4d-4d and 4d-5d Alloys.

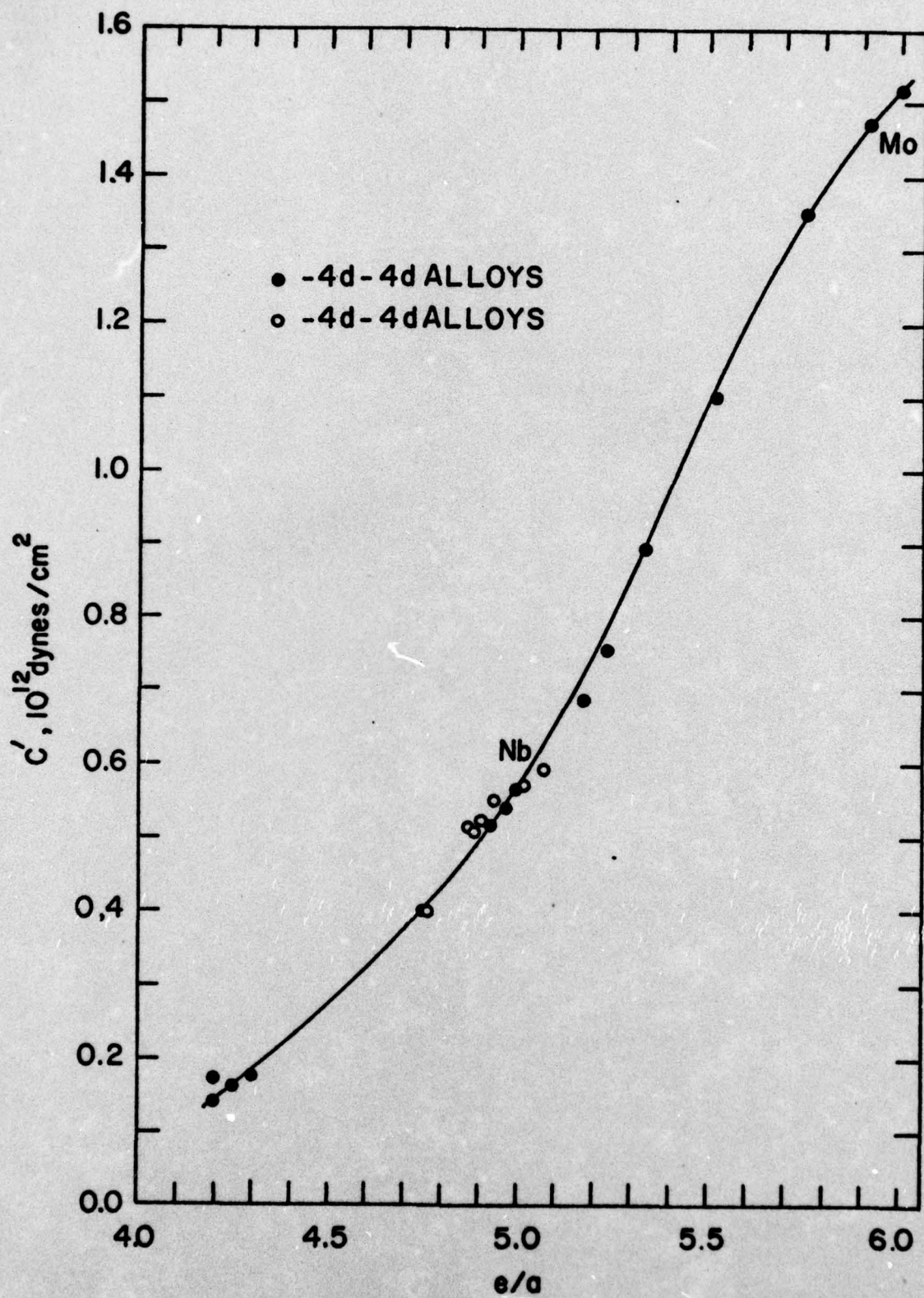


Fig. 9. C' versus e/a for 4d-4d and 4d-5d Alloys.

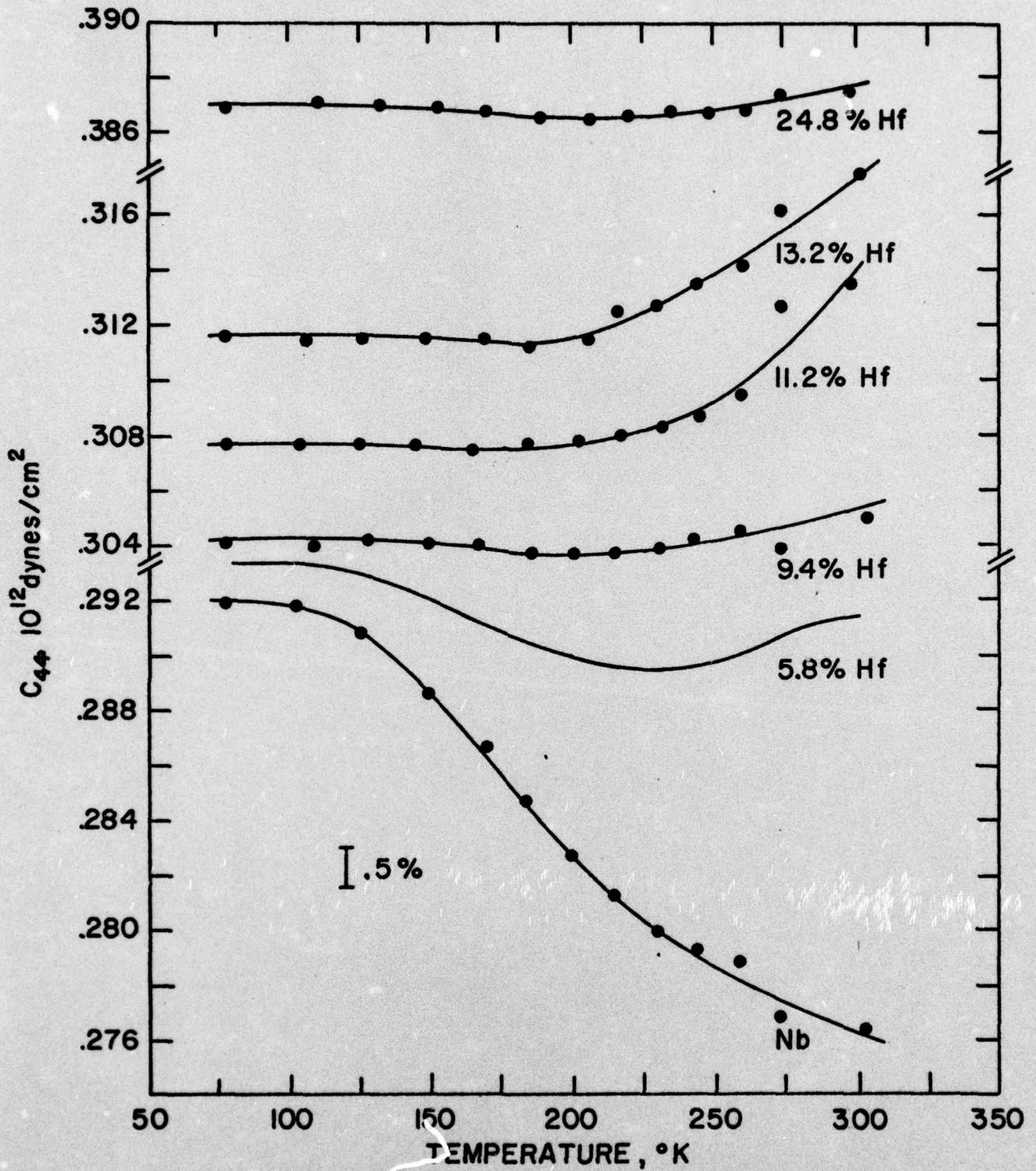


Fig. 10. Effect of Temperature on C_{44} for Nb-Hf Alloys.

Based on the work in this and other studies,^{18,19} it was found that Group VI alloying elements tend to increase C' while Group IV alloying elements tend to decrease C' as shown in Fig. 9. This indicates that decreasing the e/a ratio decreases the stability of the BCC structure while increasing the e/a ratio increases the stability of the BCC structure. This result is very significant with regard to the superconducting properties of these alloys. It is well known that a high degree of lattice instability is associated with high transition temperature (T_c) superconductors.²⁰ Since the elastic constant C' is also related to lattice stability, then there should be a correlation between the magnitude of C' and T_c . Figure 9 tends to confirm this since the addition of Group IV metals to Nb increases T_c while Group VI additions decrease T_c .²¹

The temperature dependence of the elastic constant was also determined and found to be normal for all elastic constants except for C_{44} . This anomalous behavior is shown in Figs. 10 and 11. Other studies have shown that there is a minimum in the C_{44} vs. temperature curve at approximately 450°K.²² From the present work, it appears that this minimum point is displaced to lower temperature with the addition of a Group IV alloying element. In another study,²³ it was shown that Group VI elements added to Nb displace the minimum point to higher temperature and thus it appears that this anomalous behavior is due to some electronic effect.

3. Tungsten-Tantalum Alloys

The earlier work on the W-Re alloys had determined the effect of a Group VII alloying on tungsten and this work was carried out to find the effect of a Group V element (Ta) on tungsten. The most significant finding in this phase of the study is that the curve of the elastic anisotropy ratio vs. composition follows the curve predicted by Fisher and the minimum occurs at a composition of about 55 at. % W as shown in Fig. 12. This composition should be the most stable of the Ta-W alloys because at this point the maximum value of C' as compared to C_{44} exists. This is also the most brittle alloy because a maximum in the ductile-to-brittle transition temperature occurs at this same composition.²⁴ Also it can be noted from Fig. 12 that $A = 1$ for an alloy with e/a of 5.39 which corresponds to a 39 at. % W alloy. This alloy should be suitable for high-cycle fatigue applications because it is elastically isotropic and therefore grain boundaries of a polycrystal should have only minor effects on the stress or strain distributions. The temperature dependence of all the elastic constants was normal except C_{44} of some of the alloys. In the composition range of 40-70 at. % W, C_{44} increases with increasing temperature (Fig. 13) instead of the normal behavior of decreasing with increasing temperature. The reason for this behavior is unknown but it may be due to changes in the Fermi surface that occur with temperature changes.

4. Conclusions from Elastic Constants

The results of this work provides further evidence of the relationship between the elastic properties and the electronic structure of the transition metals. This effect is especially evident in the plots of C' and A vs. the e/a ratio. It has also been shown in this study that the stability and the ductility of the BCC structure can be predicted by the magnitude of the elastic constant C' . However, it should be pointed out that the factors involved in determining whether or not a material is ductile are very complex and the elastic properties can only give an approximate prediction of the fracture behavior of a metal.

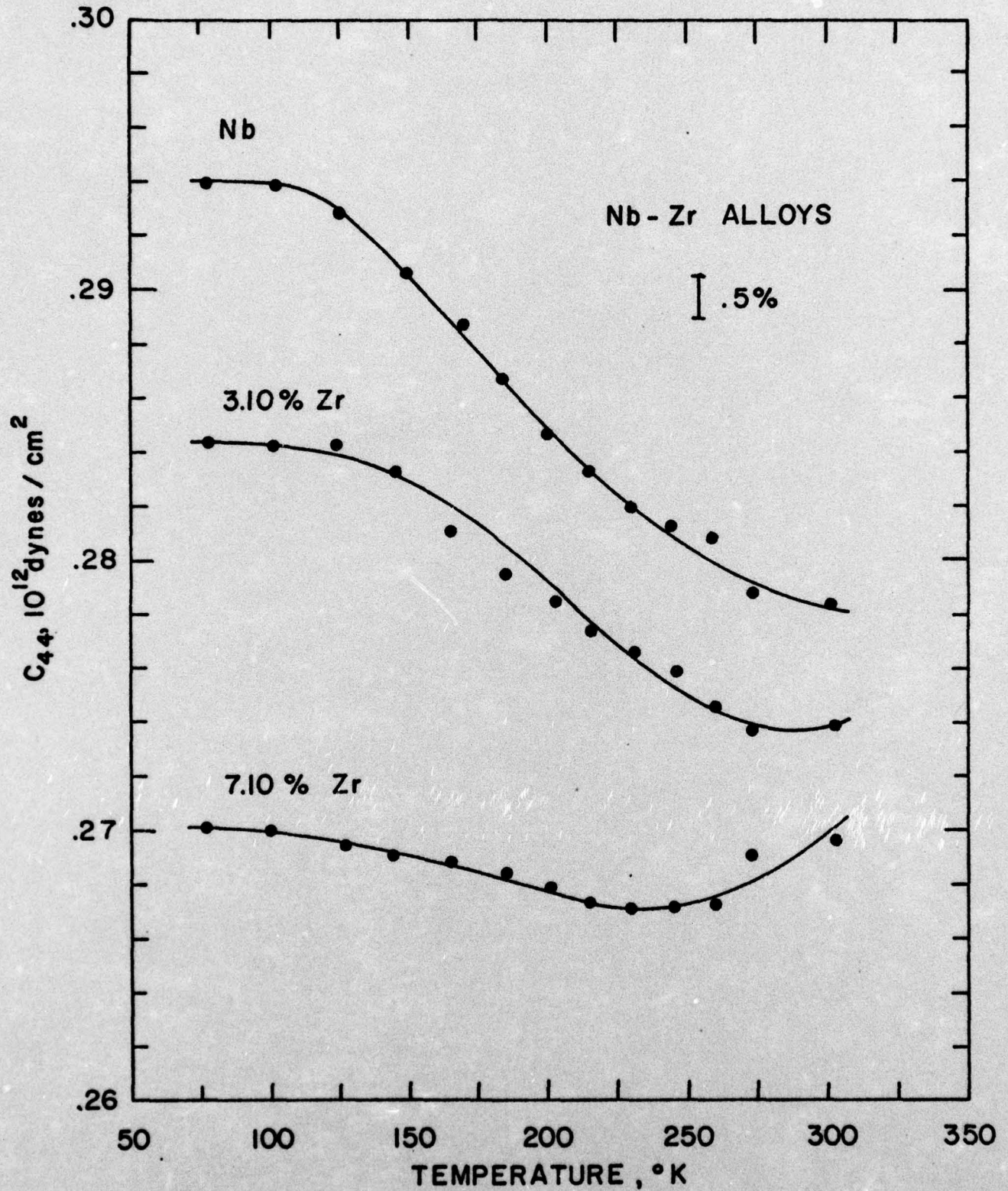


Fig. 11. Effect of Temperature on C_{44} for Nb-Zr Alloys.

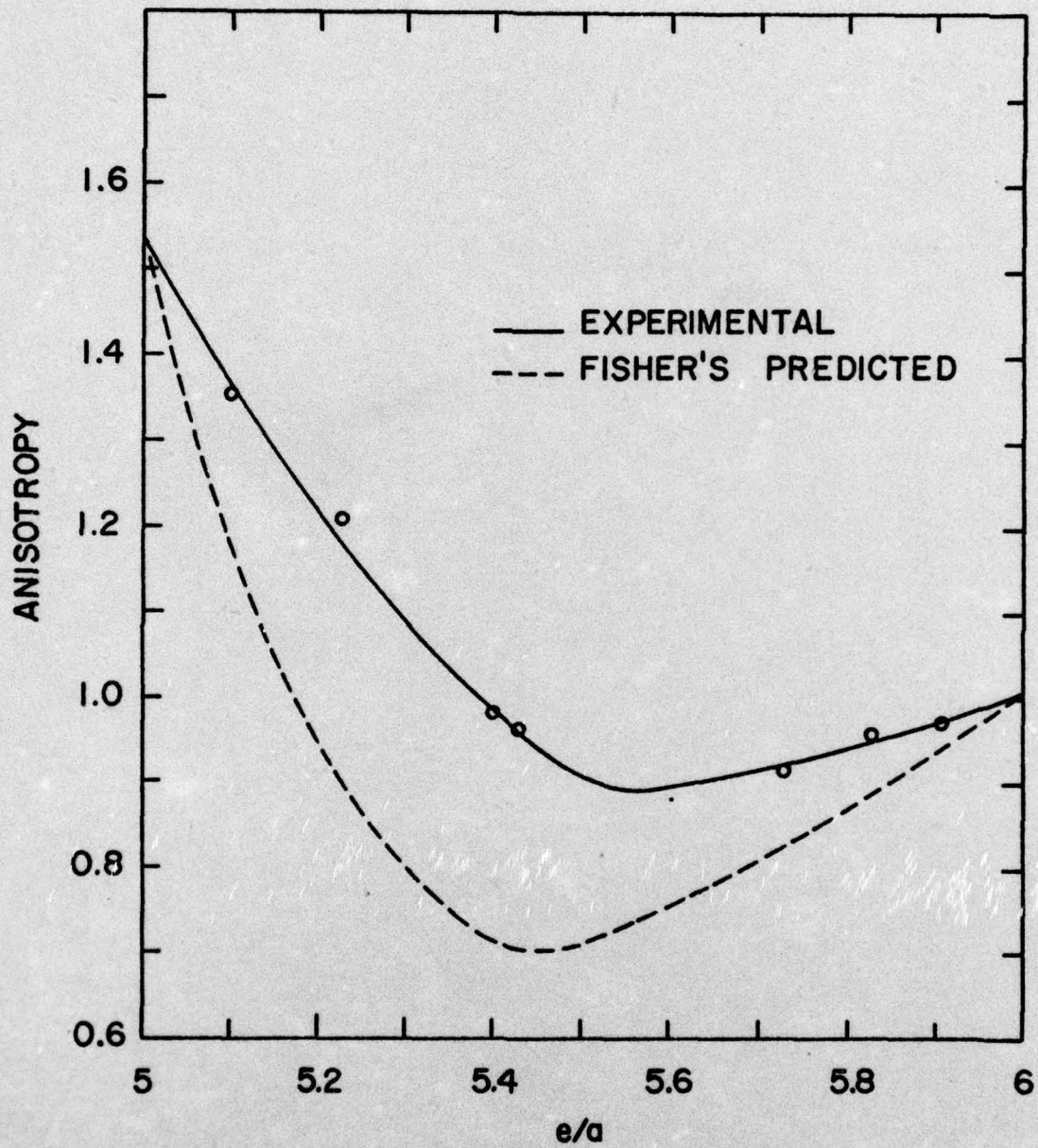


Fig. 12. Anisotropy versus e/a at 300°K for Ta-W Alloys.

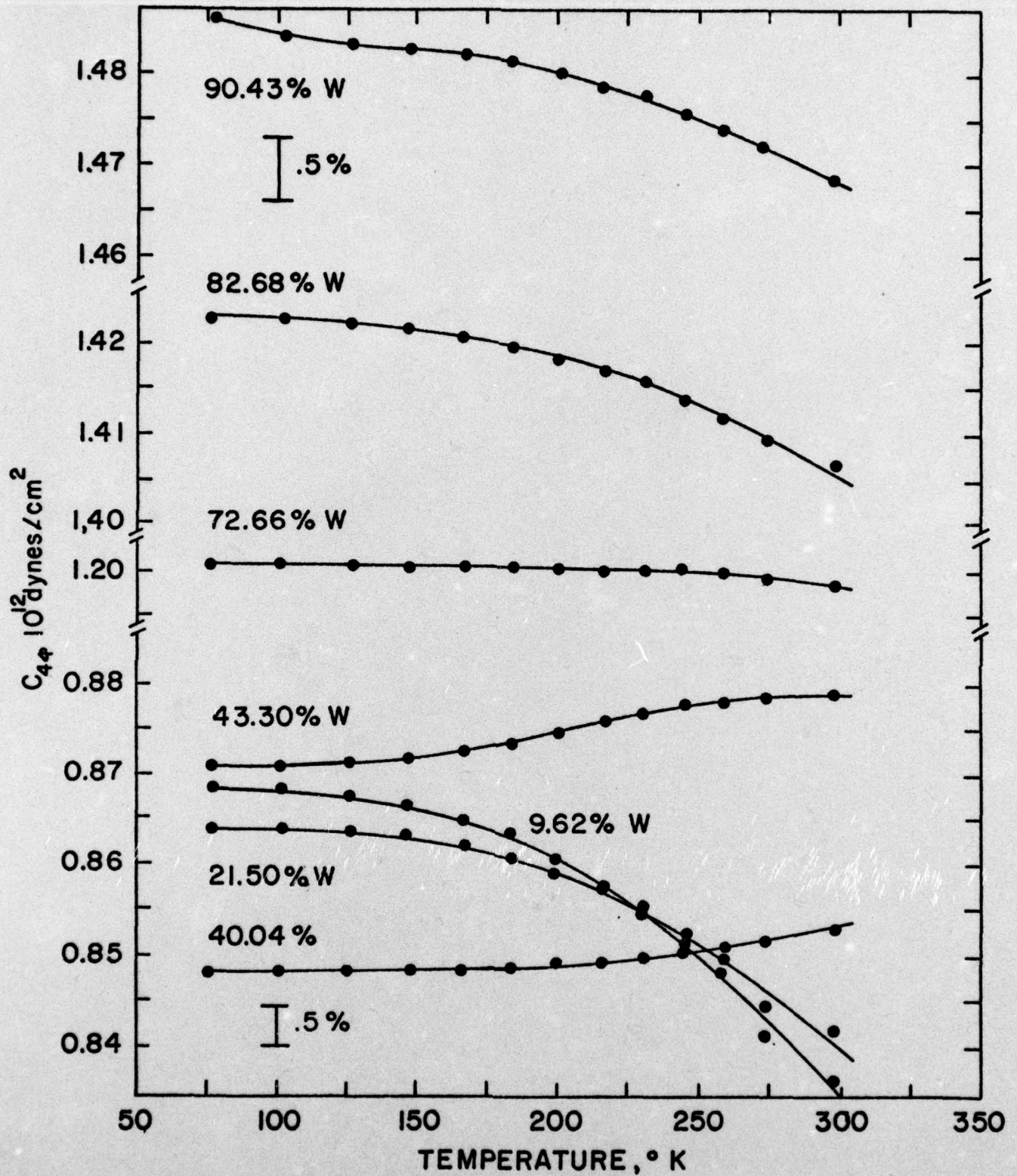


Fig. 13. Effect of Temperature on C_{44} for Ta-W Alloys.

E. Magnetic Susceptibility

In order to gain a better understanding of the electronic structure of transition metals, the magnetic susceptibility of several W-Ta was measured. This system was chosen because the elastic constant work showed that the elastic anisotropy ratio exhibited a minimum at an electron/atom ratio of about 5.5. Other investigations²⁵ have shown that some type of inflection point in the density of electronic states may be occurring at this particular e/a ratio. Since the density of states of a metal is directly related to the magnetic susceptibility, then these measurements should give an indication of any abrupt changes in the density of states with composition. The samples for these measurements were prepared here at Michigan Tech and the measurements were made at Iowa State University. The results of the room temperature measurements are listed in Table IV.

Table IV

| Magnetic Susceptibility of W-Ta Alloys | |
|--|--|
| <u>Alloy (at.%)</u> | <u>$\chi \times 10^{-6}$ emu/gm</u> |
| 25% W | 0.725 |
| 31% W | 0.710 |
| 42% W | 0.695 |
| 46% W | 0.654 |
| 50% W | 0.610 |
| 58% W | 0.488 |
| 61% W | 0.420 |
| 71% W | 0.337 |

A plot of the above data shows a very rapid decrease in χ in the composition range 40-65 at. % W. This is the same composition where the minimum in the anisotropy ratio occurs which offers further evidence of the correlation between elastic constants and the electronic structure.

F. Deformation Characteristics

Since it became clear during the course of this investigation that plastic deformation was playing an important role in the fracture behavior, a study of the effect of Re on the plastic properties of tungsten was made. Figs. 14 and 15 show the velocity of dislocation of W, W-3% Re and W-10% Re alloys as a function of stress at 298°K and 77°K respectively. These data were inferred from strain rate sensitivity tests which have been shown by Johnston and Stein²⁶, and by Schadler²⁷ to be a valid way of determining the relationship between dislocation velocity and stress. It is noted that Re is a rapid solid solution hardener of tungsten at low stress, but at high stress it is a solid solution softener. Since it is the high stress regime which is important in crack propagation, it is clear that a major role of Re in promoting ductility is a consequence of its solid solution softening at high strain rates.

Plots of the calculated plastic zones for the W and W-Re alloys at 298°K are shown in Fig. 16. These contours correspond to a dislocation velocity

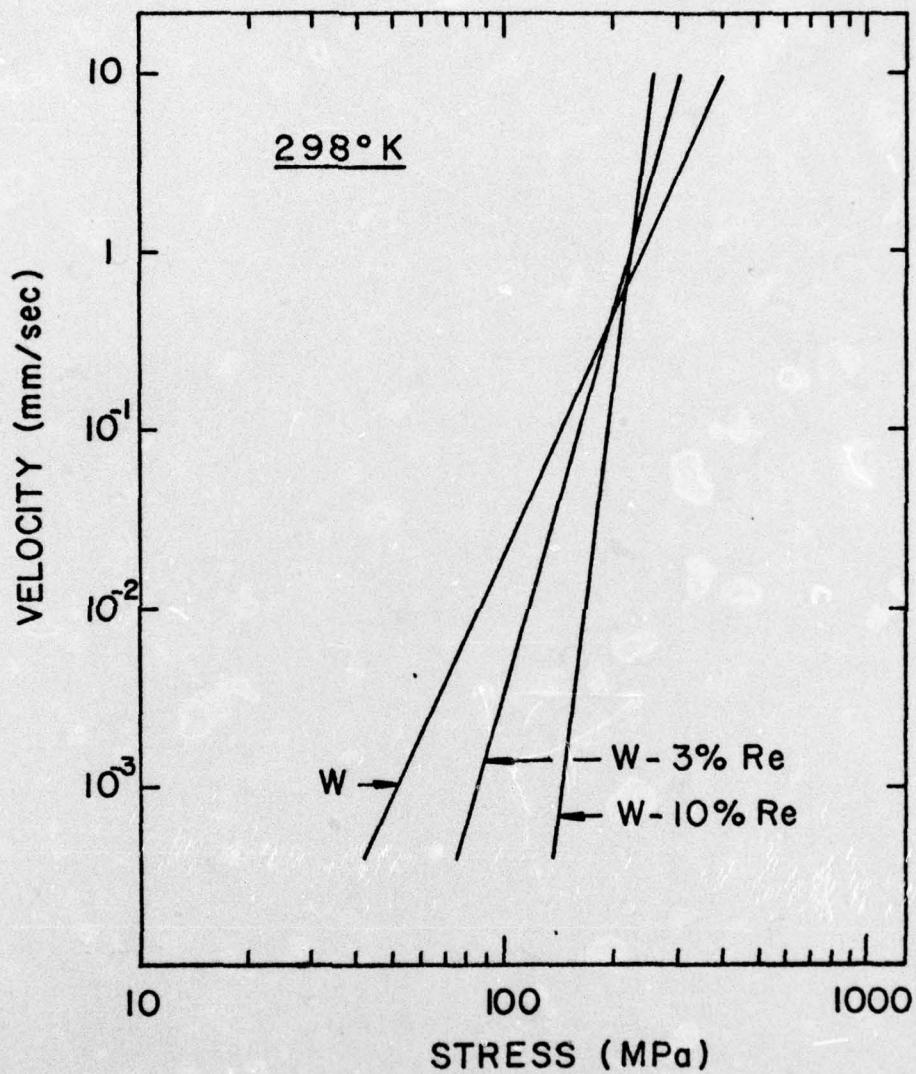


Fig. 14. Stress dependence of dislocation velocity as a function of rhenium content at 298°K. These plots are determined from the strain rate sensitivity of the proportional limit stress of single crystals.

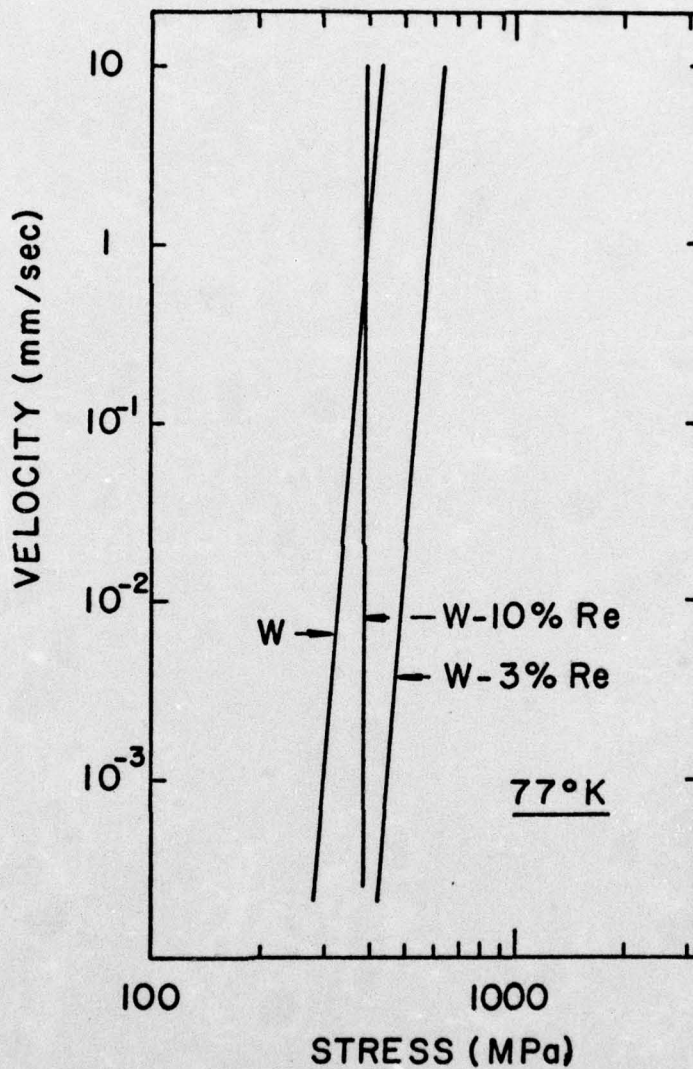


Fig. 15. Stress dependence of dislocation velocity as a function of rhenium content at 77°K . These plots are determined from the strain rate sensitivity of the proportional limit stress of single crystals.

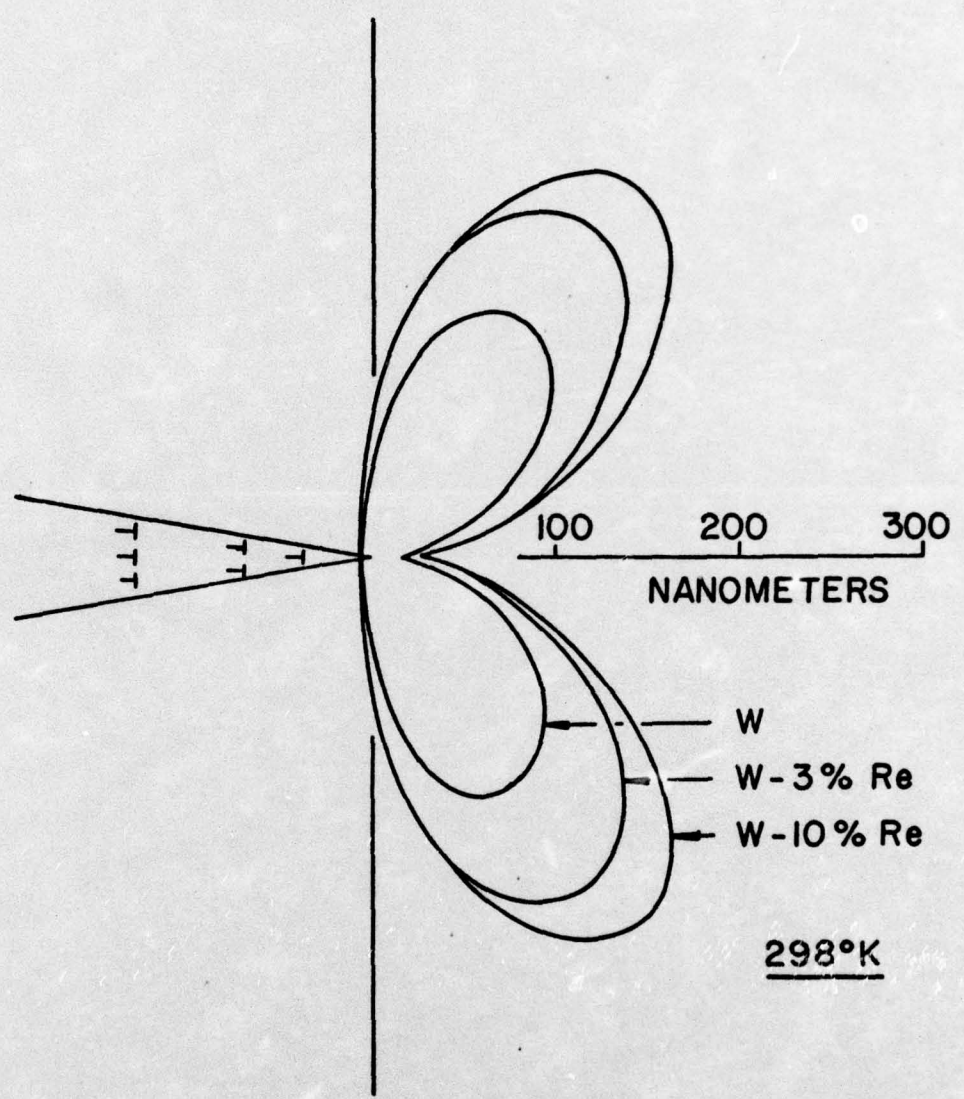


Fig. 16. Plastic zones around a crack tip as a function of rhenium content at 298°K. The contours correspond to a constant dislocation velocity of 1 cm/sec. The crack system is $\{100\}\langle 011\rangle$.

of 1 cm/sec which is the greatest velocity that can realistically be applied to the empirical relationship of Eq. (5). In a similar manner, the calculated plastic zones for the alloys at 77°K are shown in Fig. 17.

A comparison of the measured values of fracture energies in Table II with the calculated plastic zones in Fig. 16 shows qualitative agreement at room temperature. Rhenium increases both the fracture energies and the plastic zone size. In the case of W-10% Re the samples failed along a twin-matrix interface, indicating that for this composition and temperature it is more difficult to propagate a {100} cleavage crack than to separate along a twin-matrix interface. This agreement between calculations and data supports the theory that Re enhances dislocation motion at the crack tip thereby inhibiting cleavage propagation. Figure 14 demonstrates that Re decreases the strain rate sensitivity of W which increases m , the slope of the $\log V$ vs. $\log \dot{\tau}$ plot. This increase of m with Re allows dislocation motion to become "easier" relative to pure tungsten at higher strain rates resulting in a crossover point in Fig. 14 at a velocity of -1 mm/sec.

The existence of a crossover is important because it demonstrates that the faster moving dislocations, which necessarily lie closer to the crack tip, are the most effective in blunting the crack tip. Representing the plastic zone contours by another velocity greater than the crossover velocity would decrease the absolute sizes but would not alter the order of sizes. The W-10% Re composition would have the largest plastic zone and pure W the smallest.

At 77°K both the fracture energies in Table II and the calculated plastic zones in Fig. 17 decreased in magnitude relative to ambient temperature. However, the relative sizes of the calculated plastic zones with Re content are not in as good a qualitative agreement with the experimental results, especially the W-3% Re composition. The small size of this plastic zone follows from calculations based on the anomalously strong behavior of the W-3% Re samples at 77°K. It is not clear why the W-3% Re compression specimens behave in this manner at 77°K, but this result points out an important difference between deformation that is occurring at a crack tip and that which occurs throughout the bulk. That difference is the influence of the true fracture stress, σ^* , which acts as a sensitive "trigger" on the amount of deformation taking place around a crack tip. This does not appear to be as important at higher temperatures since the plastic work is sufficiently large that it can promote cleavage on the {100} plane even though the {110} plane is of lower surface energy. Consequently, the plastic zone model, based on appreciable plastic deformation, is able to predict fracture behavior with Re content at ambient temperatures but loses validity at lower temperatures where dislocation motion is difficult.

Although the relationship between the true surface energy and the plastic work surrounding a crack tip is not well understood, a simple example will help to elucidate this interaction. Assume that γ_{ijk} is proportional to the true fracture stress, σ^* , the stress required to separate atoms at the crack tip along a given plane. If σ^* is increased by 2% on the primary cleavage plane, the normal load on the crystal to induce cleavage would have to be increased. However, increasing the normal load causes a dramatic increase in the plastic strain rate, $\dot{\epsilon}_p$, at the crack tip since it is a sensitive function of shear stress.

$$\dot{\epsilon}_p \propto \tau^m$$

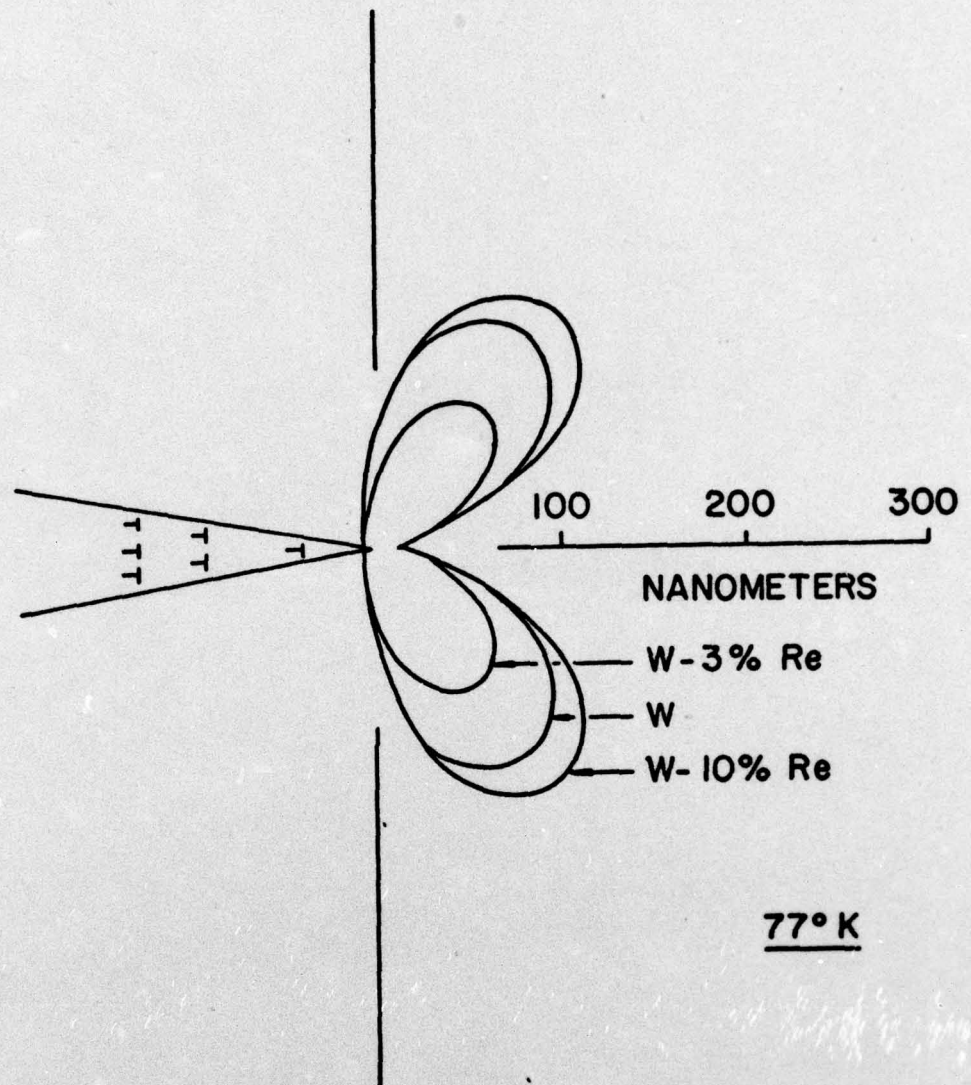


Fig. 17. Plastic zones around a crack tip as a function of rhenium content at 77°K. The contours correspond to a constant dislocation velocity of 1 cm/sec. The crack system is $\{100\}\langle 001\rangle$.

Therefore, a ratio of the two conditions (assume $m = 20$ for purposes of calculation) gives $\frac{\epsilon_{p1}}{\epsilon_{p2}} \propto (1.02)^{20} \approx 1.50$, or the plastic strain rate is 50%

greater. For a crack propagating at a constant velocity, the plastic strain will then be 50% greater, and the fracture energy will be proportionately increased. This concept of the relationship between true surface energy and plastic deformation is a departure from approaches which attempt to explain the processes controlling fracture in terms of either plastic work or γ_{ijk} .

For our samples, the measured (100) fracture energy at 77°K ranges from 3.8 J/m² for pure W to 12.6 J/m² for W-10% Re. Since γ_{100} for pure W has been measured by Cordwell and Hull²⁵ to be ~ 1.7 KJ/m², it is clear that the true surface energy plays a significant role in the cleavage fracture. It is not expected that Re markedly alters the true surface energy, but small changes in γ_{100} can drastically affect fracture energies as shown previously.

A method of estimating changes in true surface energy with Re consists of measuring changes in the elastic constants C_{44} and $C' = 1/2(C_{11} - C_{12})$. These quantities are related to the first and second nearest neighbor bonds, respectively, and therefore, contribute to the true surface energy. Following Tyson *et al*⁶ the expressions for γ_{100} and γ_{110} are shown below where ϕ_1 and ϕ_2 are the interaction potentials of first and second nearest neighbors,

$$\gamma_{100} = \frac{2\phi_1 + \phi_2}{d_0}$$

$$\gamma_{110} = \frac{\sqrt{2}(\phi_1 + \phi_2)}{d_0} \quad (7)$$

respectively, and d_0 is the lattice parameter. A plot of $\frac{\gamma_{110}}{\gamma_{100}}$ vs. $\frac{\phi_2}{\phi_1}$ is shown in Fig. 18. From measurements of C' and C_{44} at 77°K in the W-Re specimens the value of C' was found to decrease with Re additions up to W-10% Re while C_{44} increased, each by 2-3%. Thus, the $\frac{\phi_2}{\phi_1}$ would be expected to decrease, thereby decreasing the ratio $\frac{\gamma_{110}}{\gamma_{100}}$ as shown in Fig. 18. This increase of γ_{100} relative to γ_{110} with Re results in a similar increase in σ^* for the {100} plane. As stated earlier, this will produce more plastic work near the crack tip and increase the fracture energy. It is important to note that although the γ_{110} is decreasing with Re, cleavage is prohibited from propagating on this plane by the greater amount of plastic work associated with {110} cleavage. However, if the plastic work could be further suppressed in these W-Re alloys by fracturing at lower temperatures, {110} may become the preferred cleavage plane. The difficulty of promoting {110} cleavage in pure tungsten, despite its apparently lower surface energy, has already been shown by Cordwell and Hull.

The existence of twinning in the fracture samples does not conflict with the present model of plastic zones because twinning occurs after the passage

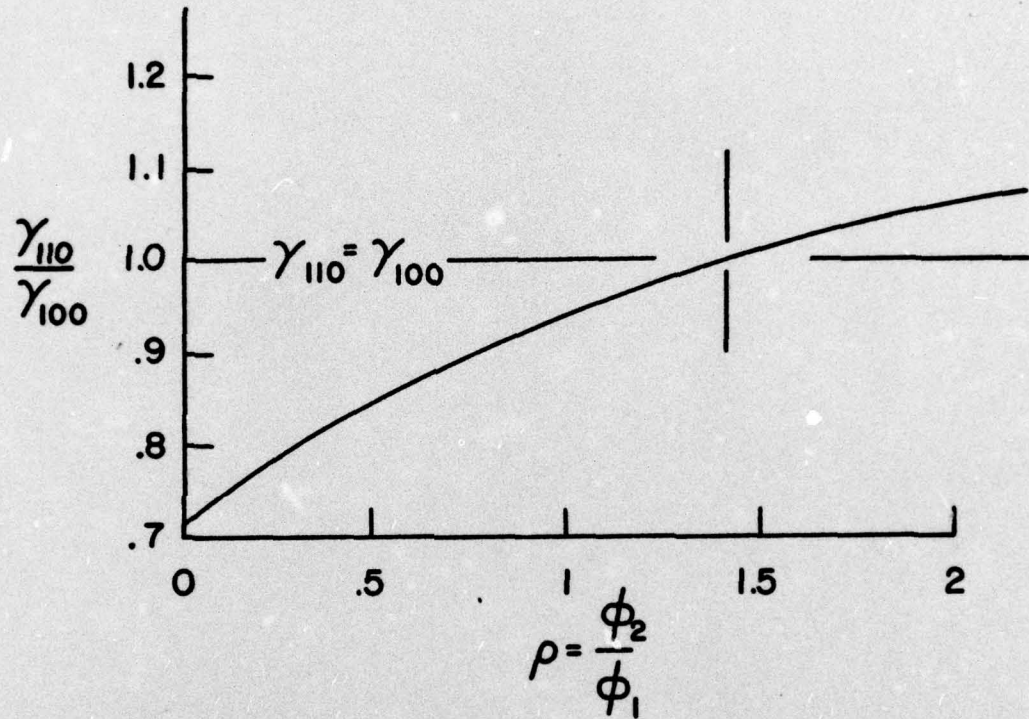


Fig. 18. Surface anisotropy with first and second nearest neighbor interactions of strength ϕ_1 and ϕ_2 .

of a crack on the (100) plane in the $\langle 100 \rangle$ direction. This crack system is expected to have the greatest velocity, and the morphology of the microtwins on the cleavage planes seems to support this prediction. If twinning had occurred in front of a (100) $\langle 100 \rangle$ cleavage crack, then the microtwins on different {112} planes would intersect and form ridges ahead of the crack front thereby eliminating any smooth $\langle 100 \rangle$ spikes. Twin ridges are only found between two close lying spikes. Since twinning is a sensitive function of slip, its presence suggests that varying amounts of slip do occur in front of the slower moving regions of the crack front. This would result in a cusp shaped crack front with the $\langle 100 \rangle$ direction leading the other directions.

REFERENCES

1. Griffith, A. A., Phil. Trans. Roy. Soc., London, A221, 163 (1920).
2. Orowan, E., Rept. Progr. in Phys. 12, 185 (1948-49).
3. Irwin, G. R., Encyclopedia of Physics, Vol. VI, Springer, Heidelberg (1958).
4. Hahn, G. T. and Gilbert, A., Technical Documentary Report No. ASD-TDR-62-1004 (1962).
5. Ayres, R. A. and Stein, D. F., Acta Met., 20, 789 (1971).
6. Tyson, W. R., Ayres, R. A., and Stein, D. F., Acta Met., 21, 621 (1973).
7. Englis, C. E., Trans. Inst. Naval Arch., London, 55, 219 (1913).
8. Born, M., Proc. Cambridge Phil. Soc., 36, 160 (1940).
9. Mie, G., Ann. Phys. Lpz. 11, 657 (1903).
10. Morse, P. M., Phys. Rev., 34, 57 (1929).
11. Johnson, R. A., Phys. Rev., 134, 1329 (1964).
12. Beardmore, P. and Hull, D. J., Inst. Met., 94, 14 (1966).
13. Geach, G. A. and Hughes, J. E., Plansee Proceedings, 1955 Metallwerw Plansee, ed. by F. Benesovsky, Pergamon Press, N.Y., 1956, p. 245.
14. Zener, C., Elasticity and Anelasticity of Metals, U. of Chicago Press, Chicago, 1948.
15. Fisher, E. S. and Dever, D., Acta Met., 18, 265, (1970).
16. Fisher, E. S., The Physics of Solid Solution Strengthening, (Materials Engineering Congress, Chicago, 1973).
17. Pugh, S. F., Phil. Mag., 45, 823 (1954).
18. Hubbell, W. C. and Brotzen, F. R., J. Appl. Phys., 43, 3306 (1972).

19. Goasdoue, C., Ho, P. S., and Sass, S. L., *Acta Met.*, 20, 725 (1972).
20. Collings, E. W., Ho, J. C., and Jaffee, R. J., *Phys. Rev. B*, 5, 4435 (1972).
21. Kulm, J. K. and Blaugher, K. D., *Phys. Rev.*, 123, 1569, (1961).
22. Graham, L. J., Nadler, H., and Chang, R., *J. Appl. Phys.*, 39, 3025 (1968).
23. Lonnee, J. E., M.S. Thesis, Michigan Technological University, 1973.
24. Ferriss, D. P., Rose, R. M., and Wulff, J., *Trans. AIME*, 224, 584 (1962).
25. Childs, B. G., Gardner, W. E., and Penfold, J., *Phil. Mag.*, 5, 1267 (1960).
26. Johnston, W. G. and Stein, D. F., *Acta Met.*, 11, 317 (1963).
27. Schadler, H. W., *Acta Met.*, 12, 861 (1964).
28. Cordwell, J. E. and Hull, D., *Phil. Mag.*, 26, 215 (1972).

Students Supported by Grant

Robert A. Ayres: Ph.D., January, 1974; thesis title: "Effect of Rhenium on the Fracture Behavior of Tungsten."

Marvin L. Carpenter: M.S., May, 1974; thesis title: "Single Crystal Elastic Constants of Ta-W Alloys."

Mary Lou Frey: M.S., May, 1974; thesis title, "Single Crystal Elastic Constants of Nb-Hf and Nb-Zr Alloys."

Roy W. Hoerauf: M.S., February, 1977; (expected) thesis title: "Relationship Between the Magnetic Susceptibility and the Elastic Constants of Ta-W Alloys."

Carl F. Musolf: M.S., January, 1975; thesis title: "Fracture Behavior of Fe-Si and Determination of Optimum Interatomic Potential for Ideal Strength Calculations."

Publications

"Low Temperature Brittleness," D. F. Stein, Keynote Paper, Proceedings of Third International Conference on the Strength of Metals and Alloys, Vol. II, 58-89, 1974.

"Elastic Constants of Tungsten Rhenium Alloys from 77 to 298°K," R. A. Ayres, G. W. Shannette, and D. F. Stein, *J. of Appl. Phys.*, 46, 1526, April, 1975.

Manuscripts in Preparation

"Effect of Rhenium on the Fracture Behavior of Tungsten," R. A. Ayres and D. F. Stein.

"Elastic Constants of Niobium-Zirconium, Hafnium, and Tungsten Alloys," M. L. Frey, J. E. Lonnee, and G. W. Shannette.

List of Figure Captions

- Figure 1. Model of a Partially Relaxed Crack. Hahn and Gilbert⁴
- Figure 2. Calculated Stress Concentration α for an Elliptical Crack, Length $2a$ and Root Radius r , as a Function of Distance. Hahn and Gilbert⁴
- Figure 3. Schematic Presentation of Stress and Strain Ahead of a Moving Crack. Hahn and Gilbert⁴
- Figure 4. Schematic of Potential Function and Force Function for One-Dimensional Crystal.
- Figure 5. (100) Fracture Surface of W-3% Re tested at 298°K. The smooth $\langle 100 \rangle$ spike is shown originating from precrack. Coarse microtwins lay parallel to the $\langle 110 \rangle$ direction. 60X
- Figure 6. The elastic constant $C' = 1/2 (C_{11} - C_{12})$ as a function of rhenium content for different temperatures.
- Figure 7. The elastic constant C' for Nb-Hf and Nb-Zr alloys.
- Figure 8. Anisotropies of 4d-4d and 4d-5d alloys.
- Figure 9. C' versus e/a for 4d-4d and 4d-5d alloys.
- Figure 10. Effect of temperature on C_{44} for Nb-Hf alloys.
- Figure 11. Effect of temperature on C_{44} for Nb-Zr alloys.
- Figure 12. Anisotropy versus e/a at 300°K for Ta-W alloys.
- Figure 13. Effect of temperature on C_{44} for Ta-W alloys.
- Figure 14. Stress dependence of dislocation velocity as a function of rhenium content at 298°K. These plots are determined from the strain rate sensitivity of the proportional limit stress of single crystals.
- Figure 15. Stress dependence of dislocation velocity as a function of rhenium content at 77°K. These plots are determined from the strain rate sensitivity of the proportional limit stress of single crystals.
- Figure 16. Plastic zones around a crack tip as a function of rhenium content at 298°K. The contours correspond to a constant dislocation velocity of 1 cm/sec. The crack system is $\{100\}\langle 011 \rangle$.
- Figure 17. Plastic zones around a crack tip as a function of rhenium content at 77°K. The contours correspond to a constant dislocation velocity of 1 cm/sec. The crack system is $\{100\}\langle 011 \rangle$.
- Figure 18. Surface anisotropy with first and second nearest neighbor interactions of strength ϕ_1 and ϕ_2 .